

Article

# Effects of Al Sputtering Film on the Oxidation Behavior of NiCrAlY Bondcoat

Yong Zhang <sup>1,2,3</sup>, Gengfei Zhang <sup>1</sup>, Qiang Yang <sup>4</sup>, Weicheng Cao <sup>3</sup>, Jian Pu <sup>5</sup> and Chao Zhu <sup>6,\*</sup> 

<sup>1</sup> School of Material Science and Engineering, Chang'an University, Xi'an 710064, China; chdzhangyong@chd.edu.cn (Y.Z.); zhanggfchd@126.com (G.Z.)

<sup>2</sup> Department of Chemistry and Materials Engineering, University of Auckland, Auckland 1142, New Zealand

<sup>3</sup> Technical Center, Jinduicheng Molybdenum Co., Ltd., Xi'an 710077, China; weichengcao5876@163.com

<sup>4</sup> Three places of Technology, Northwest Industrial Group Co., Ltd., Xi'an 710043, China; yq19841112abc@163.com

<sup>5</sup> State Key Laboratory of Materials Processing and Die & Mould Technology, Huazhong University of Science and Technology, Wuhan 430074, China; hzpujian@126.com

<sup>6</sup> Science and Technology on Thermostructural Composite Materials Laboratory, Northwestern Polytechnical University, Xi'an 710072, China

\* Correspondence: chaozhu30@gmail.com

Received: 17 March 2020; Accepted: 8 April 2020; Published: 10 April 2020



**Abstract:** In this study, the oxidation behavior of Al coated NiCrAlY bondcoat is investigated. It is known that many methods are applied to improve the lifetime of bondcoat in thermal barrier coatings. Herein, the Al sputtering method is selected to increase the Al content, which does not change the structure of bondcoat. Thin Al film of ~2  $\mu\text{m}$  was sputtered on the surface of bondcoat, which improved the oxidation resistance of NiCrAlY bondcoat. Experimental results showed that, after oxidation for 200 h at 1200 °C, the formation of a dense and continuous  $\alpha\text{-Al}_2\text{O}_3/\text{Cr}_2\text{O}_3$  multilayer was observed on the Al coated bondcoat surface. In contrast, a mixed oxides (NiO,  $\text{Cr}_2\text{O}_3$  and spinel oxides) layer formed on the surface of the as-sprayed bondcoat samples. Results of the cyclic oxidation at 1050 °C within 204 h indicated that the Al sputtering method can improve the oxidation resistance of bondcoat. This study offers a potential way to prolong the lifetime of thermal barrier coatings and provides analysis of the oxidation mechanism.

**Keywords:** NiCrAlY bondcoat; Al film; sputtering; oxidation resistance

## 1. Introduction

Thermal barrier coatings (TBCs) are widely employed to thermally protect gas turbine engines. The detailed functions of TBCs include the improvement of the efficiency, durability, and properties in high temperature operation environments [1–4]. TBCs generally comprise three layers, including a ceramic topcoat, an interlayer bondcoat, and a superalloy substrate. It has been proven that TBCs are used in the hot sections as an important component in protecting the gas turbines from oxidation, thermal fatigue, corrosion, wear, and erosion [5–8].

The load-carrying substrate is typically the Ni-based superalloy. The state of art topcoat material is 6–8 wt.% yttria-stabilized zirconia (YSZ) ceramic coating, which provides the advantages of low thermal conductivity, high thermal-expansion coefficient, and high fracture toughness [9–11]. YSZ topcoat can be deposited by mainly two methods: electron beam physical vapor deposition (EB-PVD) and air plasma spray method (APS) [12–14]. Interlayer bondcoat is between bond topcoat and substrate, which protects the superalloy substrate from being oxidized in severe environments and serves the critical role of providing adhesion between the substrate and the topcoat [15,16]. Two kinds of bondcoat are widely used in the TBCs system [1,2,6]: one is overlay bondcoat such as MCrAlY (M = Ni and/or

Co) bondcoat, and the other is diffusion bondcoat such as Pt/Al diffusion coating [17,18]. In Pt/Al coatings, the aluminum is required in the pack process or in the chemical vapor deposition (CVD) reactor from an  $\text{AlCl}_3$  source [2,19]. Thicker bondcoats can be achieved during the thermal spray process compared with Pt/Al bondcoats with the aluminizing process, as thermal spray process does not involve the diffusion [1,2,20].

At elevated temperatures, oxygen penetrates “oxidation transparent” YSZ topcoats to contact the bondcoats [2,9]. Oxygen goes through the microstructural defects in topcoats such as pores, voids, splat boundaries, lamellar interfaces, and cracks; while diffuses through the crystal defects due to the oxygen vacancies in YSZ. Therefore, thermally grown oxides (TGO) form between the original topcoat/bondcoat interface [21–24]. Ideal TGO is a continuous and dense  $\alpha\text{-Al}_2\text{O}_3$  layer, which plays the role of diffusion barrier to suppress the formation of detrimental oxides during further oxidation, thus improving the durability of the TBCs system under thermal exposure in service. However, some minor oxides, such as  $\text{Cr}_2\text{O}_3$ , NiO, and spinel oxides are also formed and mixed along the  $\alpha\text{-Al}_2\text{O}_3$  layer. These scales with mixed oxides thicken during oxidation, which is the main cause for the separation of the coatings from superalloy substrate, leading to the failure of TBCs [21–24]. Some transient oxide products, such as  $\theta\text{-Al}_2\text{O}_3$ ,  $\gamma\text{-Al}_2\text{O}_3$ , and  $\delta\text{-Al}_2\text{O}_3$ , can initially form on the surface of MCrAlY bondcoats [25–27]. Through heat treatment, volume expansion occurs in these metastable phases during the  $\alpha\text{-Al}_2\text{O}_3$  phase transformation [2,25–27]. For example, the volume change from  $\theta\text{-Al}_2\text{O}_3$  to  $\alpha\text{-Al}_2\text{O}_3$  can be as much as 12% [2], which may lead to cracks in TGOs and degrade the TBCs [28–30]. Therefore, the oxidation resistance and lifetime of TBCs can be improved with the formation of pure  $\alpha\text{-Al}_2\text{O}_3$  layer on the surface of bondcoat during oxidation.

Al content increase in the bondcoats is an effective way to prevent the formation of mixed oxides and metastable aluminas. It is known that some methods, such as pack cementation, CVD, PVD, sputtering, and laser treatment, are widely used to increase the content of Al in bondcoats [31–34]. For example, an improvement of oxidation resistance was achieved by coating a  $\sim 3\ \mu\text{m}$  Al film on the surface of NiCr alloy, followed by a diffusion process which heated the samples at  $600\ ^\circ\text{C}$  and then  $900\ ^\circ\text{C}$  in argon gas atmosphere. The results of cyclic oxidation at  $1100\ ^\circ\text{C}$  indicated that the weight gain data of coated samples are smaller than those of uncoated Al NiCr alloy. This is due to the formation of  $\alpha\text{-Al}_2\text{O}_3$  layer on the coated sample and the formation of  $\text{Cr}_2\text{O}_3$  layer on the uncoated sample [32]. Under  $1100\ ^\circ\text{C}$ ,  $\alpha\text{-Al}_2\text{O}_3$  layer has better oxidation resistance compared with  $\text{Cr}_2\text{O}_3$  layer [32]. This study is based on the NiCr alloy rather than the bondcoat in TBCs system. Thus, it is necessary to investigate that the effect of Al film on the bondcoat.

In this study, with the aim to increase the Al content, a thin Al film was sputtered on the surface of NiCrAlY bondcoat. This helps to the formation of a dense and continuous  $\alpha\text{-Al}_2\text{O}_3$  layer, while prevents the formation of mixed oxides (NiO,  $\text{Cr}_2\text{O}_3$  and spinel oxides). The oxidation behavior of uncoated and coated NiCrAlY bondcoats are investigated and discussed.

## 2. Materials and Methods

### 2.1. Sample Preparation

Inconel 738 coupons ( $25 \times 25 \times 5\ \text{mm}^3$ ) were used as substrates. First, both sides of coupons were polished down to  $5\ \mu\text{m}$ . Then, grit blast was conducted by alumina ( $800\ \mu\text{m}$ ) on both surfaces of samples. Finally, samples were ultrasonically cleaned with alcohol. Second, NiCrAlY bondcoats are deposited on both sides of coupons using air plasma spraying method (Praxair 3710, Praxair Inc., Cleveland, OH, USA). Commercial NiCrAlY (KF-343) feedstock was purchased from BGRIMM Tech. Group, Beijing, China. Table 1 shows the properties of NiCrAlY powders. Table 2 presents details of the APS processing conditions. The thickness of sprayed NiCrAlY bondcoat is  $150 \pm 20\ \mu\text{m}$ .

**Table 1.** Size distributions and compositions of NiCrAlY powders.

Powder	Nominal Particle Size Distributions D (0.1)–D (0.9)	Average Particle Sizes D (0.5)	Compositions (wt.%)
NiCrAlY powder	10.0–40.0 $\mu\text{m}$	25.0 $\mu\text{m}$	69Ni–20Cr–10Al–1Y

**Table 2.** Air plasma spray processing parameters.

Parameter	Unit	NiCrAlY Feedstocks
Gun nozzle inner diameter	mm	6
Arc current	A	600
Arc voltage	V	70
Primary gas flow rate (Ar)	L/min	80
Secondary gas flow rate (H <sub>2</sub> )	L/min	6
Carrier gas flow rate (Ar)	L/min	10
Gun traverse speed	mm/s	800
Powder feed rate	g/min	40
Spray distance	mm	100

## 2.2. Al Sputtering Process

Direct current magnetron sputtering technique is used to produce the Al film, which was coated on the surface of NiCrAlY bondcoat. The details of the sputtering conditions are shown in Table 3. The thickness of Al film coated on the surface of NiCrAlY bondcoat was  $\sim 2 \mu\text{m}$ , which was estimated from processing parameters.

**Table 3.** Sputtering conditions on the surface of NiCrAlY bondcoat.

Substrate	Unit	NiCrAlY Bondcoat
Target	/	Al (99.9%)
Target size	$\text{mm}^3$	$320 \times 200 \times 6$
Substrate to target distance	mm	50
Pre-sputtering time	min	20
Working pressure	Pa	0.16
DC power	W	25
Ar flow rate	mL/min	23
Deposition time	min	20
Al coating thickness	$\mu\text{m}$	$\sim 2$

## 2.3. Oxidation

Isothermal oxidation test was conducted at 1200 °C in static air at atmospheric pressure, the as-sprayed and Al coated NiCrAlY samples were heated for 1 h, 5 h, and 200 h. Thermal cycling oxidation test was performed at 1050 °C for 204 h. By measuring weight gains of samples, the oxidation behavior of as-sprayed and Al coated NiCrAlY samples was evaluated. One thermal cycle of 12 h consisted of 15 min ramp-up, 11 h isothermal soak at 1050 °C, and 45 min cool-down to ambient temperature ( $\sim 25 \text{ }^\circ\text{C}$ ). The weight measurements were taken after each cooling cycle. The precision of the measuring balance was  $\pm 0.1 \text{ mg}$ .

The oxidation kinetics of bondcoats can be quantified by the value of weight change per unit area at a certain high temperature [18,22,24,32,33,35]. The pattern of kinetics curve generally shows a parabolic weight gain behavior in the main process of oxidation, followed by a weight loss ending which corresponds to a failure period in TBCs system.

## 2.4. Sample Characterization

Scanning electron microscopy (SEM, JSM-7000F, Tokyo, Japan) in second electron mode and back scattered electron mode was used to observe the surface and cross-sectional morphologies of as-sprayed and Al coated NiCrAlY samples. X-ray spectroscopy (EDX) was used to examine

the chemical composition of the samples. The mean area and length of TGO scale were measured using ImageJ software. A series of SEM images were obtained for each sample with a magnification of 1000 $\times$ . The resolution of these images was 600 dpi. Moreover, twenty images were randomly chosen from the cross-section of each sample. The X-ray diffraction (XRD, Philips X'pert, Amsterdam, Netherlands, Cu K $\alpha$  radiation, 45 kV, 40 mA) method was used to identify the phases of oxidized samples. All XRD patterns were recorded by running X-ray diffractometer the condition of scan step = 0.02 $^\circ$  and 2 $\theta$  = 20–80 $^\circ$ .

### 3. Results

#### 3.1. Microstructure of as-Sprayed and Al Coated NiCrAlY Bondcoat Samples

In Figure 1, the cross-section of as-sprayed NiCrAlY bondcoat on the Inconel 738 superalloy substrate is shown. It can be observed that the total thickness of NiCrAlY bondcoat is  $\sim$ 150  $\mu\text{m}$ , which contact the Ni-based substrate tightly. In addition, microcracks and voids are produced during the spray process, showing the non-fully dense morphology. Moreover, the air plasma sprayed process also introduces the formation of Al<sub>2</sub>O<sub>3</sub> oxides. These segmented Al<sub>2</sub>O<sub>3</sub> veins are unevenly dispersed in the NiCrAlY bondcoat [18,36].

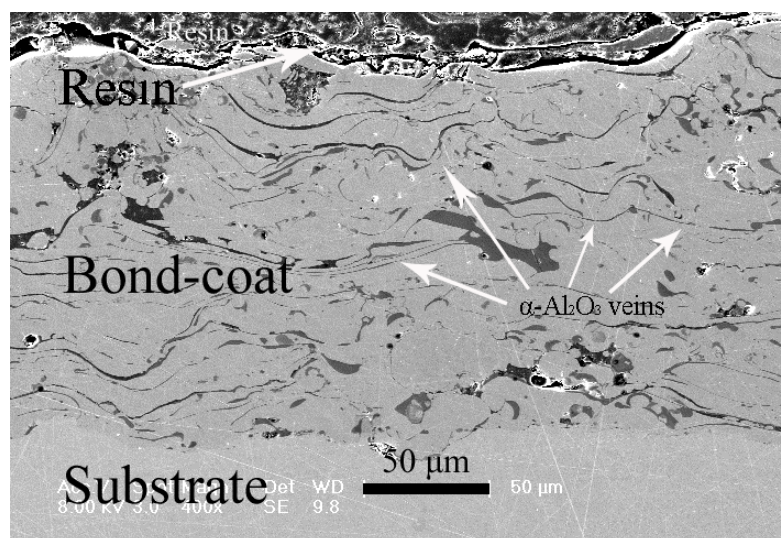
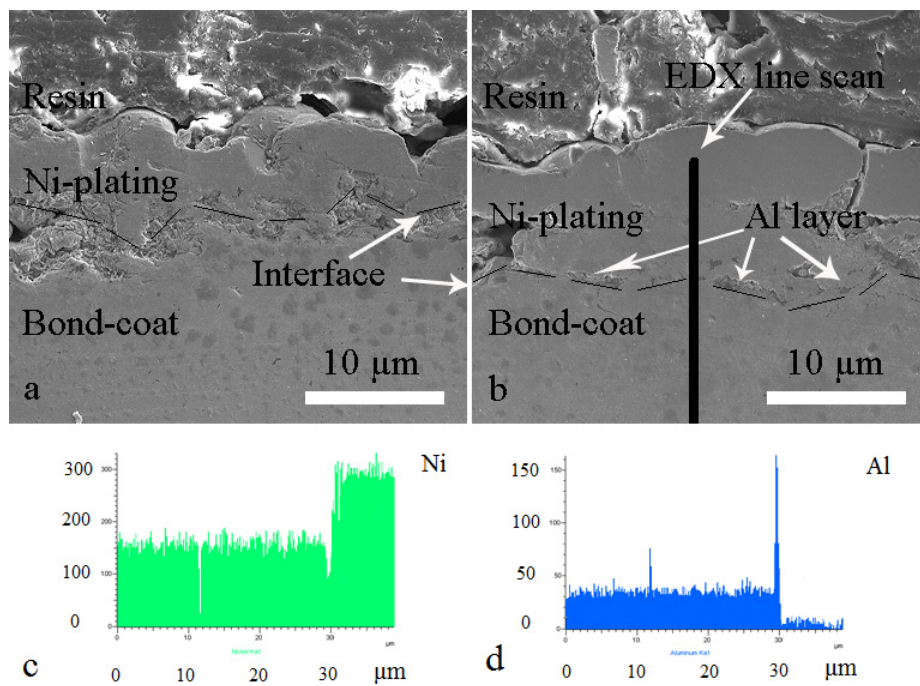


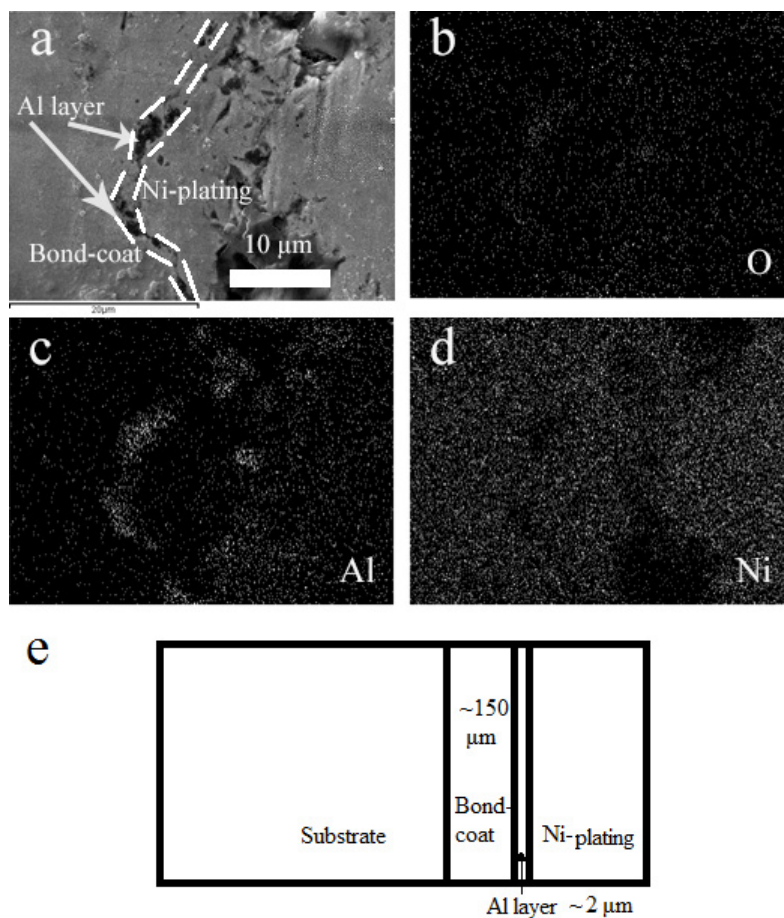
Figure 1. Cross-sectional morphology of the as-sprayed APS bondcoat.

To observe clearly the interface morphology of bondcoat/Al coat, the cross-sectional SEM images of as-sprayed sample (Figure 2a) and Al coated sample (Figure 2b) at higher magnification compared with Figure 1 are presented. Bondcoat/Ni-plating interfaces are marked by dashed line. The Al layer in Figure 2b is labeled. EDX line scan results along the marked black line in Figure 2b of Ni and Al element are presented in Figure 2c,d, respectively. The Al peak shown in Figure 2d indicates corresponded Al layer between bondcoat and Ni-plating in Figure 2b.

From Figure 3, it can be seen that Al film was successfully deposited on the surface of NiCrAlY bondcoat samples. Figure 3a shows the correctional morphology at higher magnification of Al/NiCrAlY interface as compared to Figure 2b. The elemental maps (O, Al and Ni) of the Al/NiCrAlY coating correspond to Figure 3a are presented in Figure 3c–e. In Figure 3c, the sputtered Al film of  $\sim$ 2  $\mu\text{m}$  on the surface of NiCrAlY bondcoat can be confirmed by the scattered bright Al particles. However, it can be seen that the bright O zone is not as clear as Al zone in Figure 3b. This indicates that the sputtered Al is not heavily oxidized. Figure 3e is the schematic showing the layers and thickness of each layer.



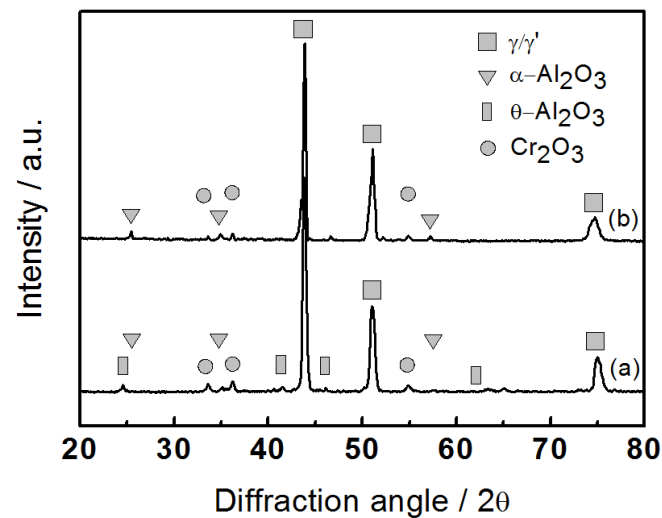
**Figure 2.** Cross-sectional view of SEM micrographs of NiCrAlY bondcoat (a) as-sprayed sample, (b) Al coated sample. EDX line scan profile of (c) Ni and (d) Al, showing the Al layer.



**Figure 3.** (a) Cross-sectional morphology of Al coated bondcoat; (b) elemental map contrast of O; (c) elemental map contrast of Al; (d) elemental map contrast of Ni and (e) a schematic of (a) showing the layers of the Al coated sample.

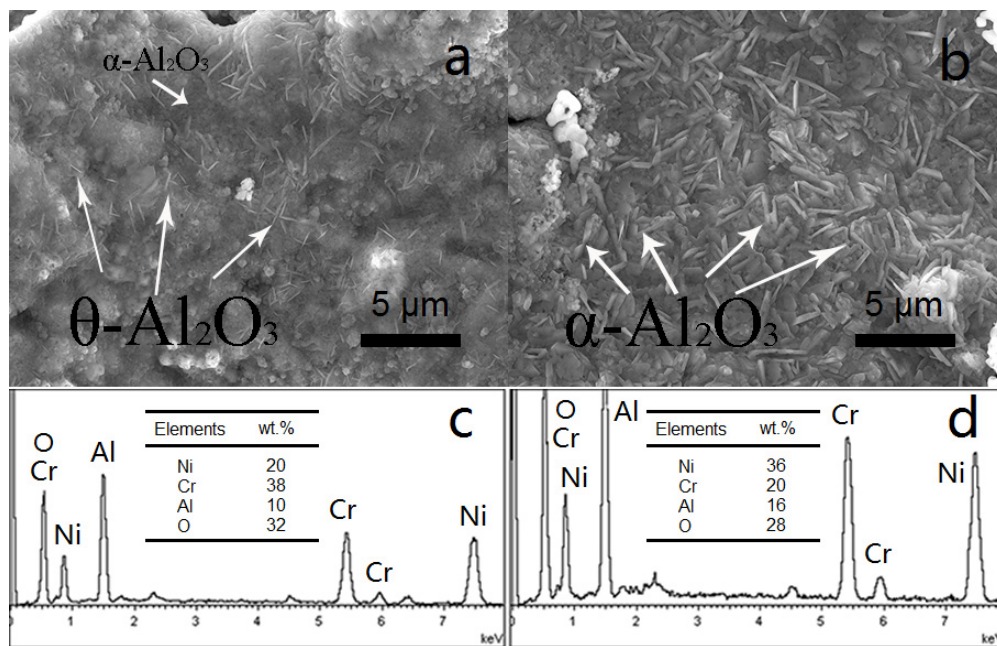
### 3.2. NiCrAlY Bondcoat Samples after Isothermal Oxidation for 1 h at 1200 °C

Figure 4 presents the XRD spectra of as-sprayed and Al coated NiCrAlY bondcoat samples after the isothermal oxidation for 1 h at 1200 °C. The XRD results show that the  $\text{Cr}_2\text{O}_3$  phase is found on both the surface of as-sprayed and Al coated samples (Figure 4a,b). In addition, both  $\theta\text{-Al}_2\text{O}_3$  and  $\alpha\text{-Al}_2\text{O}_3$  phase is observed in as-sprayed bondcoat samples, while only  $\alpha\text{-Al}_2\text{O}_3$  phase is investigated in Al coated bondcoat samples. It is noted that the intensity of the  $\alpha\text{-Al}_2\text{O}_3$  peaks of as-sprayed sample is smaller than that of Al coated sample. From Figure 4, it can be concluded that  $\theta\text{-Al}_2\text{O}_3$  phase is only detected in the as-sprayed sample and the intensity of  $\alpha\text{-Al}_2\text{O}_3$  phase is stronger in the Al coated sample.



**Figure 4.** XRD spectra of the bondcoat samples after oxidation for 1 h at 1200 °C (a) as-sprayed sample, (b) Al coated sample.

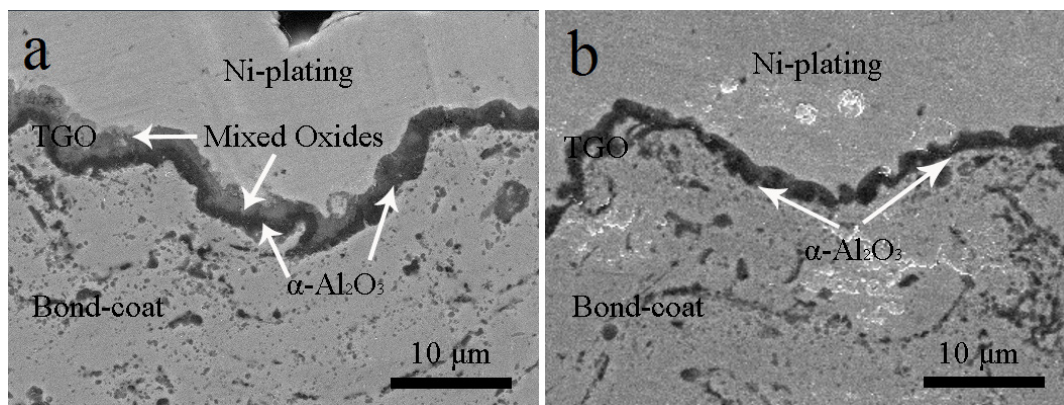
The surface morphology of the as-sprayed and Al coated NiCrAlY bondcoat samples after isothermal oxidation for 1 h at 1200 °C is shown in Figure 5a,b, respectively. Some protrudes, pores, and pits are observed in the fine oxide particles on the surface of samples. EDX spectra were obtained from the whole surface of samples. Results in Figure 5c,d show that strong Al and Cr peaks can be found, indicating that the oxides are mainly Al and Cr oxides. Ni peaks correspond to the Ni oxides. From Figure 4, it is confirmed that both  $\theta\text{-Al}_2\text{O}_3$  and  $\alpha\text{-Al}_2\text{O}_3$  phase are observed in as-sprayed sample, while only  $\alpha\text{-Al}_2\text{O}_3$  phase is found in Al coated sample. From Figure 5, the oxides are identified/speculated from their typical morphology reported in earlier works and EDX data. In Figure 5a, it can be seen that whisker like/blade-like oxides  $\theta\text{-Al}_2\text{O}_3$  form dominantly on the surface of as-sprayed bondcoat samples [25,26,33] with minor web like or dense equiaxed structure oxides  $\alpha\text{-Al}_2\text{O}_3$  [25,27], while in Figure 5b, only web like or dense equiaxed structure oxides  $\alpha\text{-Al}_2\text{O}_3$  can be observed. EDX spectra in Figure 5c,d indicate that the Al content may increase in the as-sprayed bondcoat compared with that of Al coated bondcoat.



**Figure 5.** Surface morphology of the bondcoat samples after oxidation for 1 h at 1200 °C (a) as-sprayed sample, (b) Al coated sample; and EDX spectrum (c) as-sprayed sample, (d) Al coated sample.

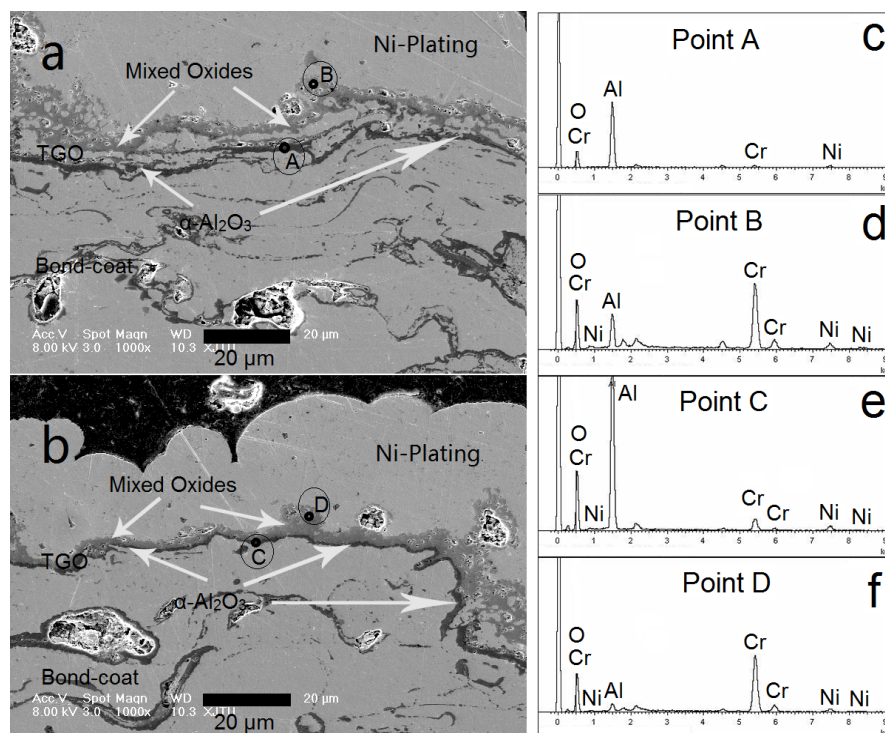
### 3.3. NiCrAlY Bondcoat Samples after Isothermal Oxidation at 1200 °C

Figure 6a,b shows the cross-sectional SEM image of as-sprayed and Al coated samples after oxidation at 1200 °C for 5 h, respectively. The TGO layer is formed on the surface of NiCrAlY bondcoats for both samples. The thickness of the TGO of the as-sprayed bondcoat sample is in the range of ~1.7~4.2  $\mu\text{m}$ , while the thickness of the TGO of Al coated bondcoat sample is in the range of ~1.2~1.7  $\mu\text{m}$ . Moreover, the average thickness of the TGO of as-sprayed sample is ~3.6  $\mu\text{m}$ , while that of Al coated bondcoat sample is ~1.4  $\mu\text{m}$ .



**Figure 6.** Cross-sectional morphology of bondcoat samples after oxidation for 5 h at 1200 °C (a) as-sprayed sample, (b) Al coated sample.

The cross-sectional morphology of as-sprayed and Al sputtered NiCrAlY bondcoat samples are shown in Figure 7a,b, respectively. After isothermal oxidized at 1200 °C for 200 h, TGO forms on the surface of bondcoat in both samples. In Figure 7a,b, four sites A, B, C, and D are marked on the TGOs in the SEM images. These sites are the areas used to measure the compositions of Al, Cr, and Ni by EDX showing in Table 4. In addition, Figure 7c–f presents the EDX spectra of corresponding areas.



**Figure 7.** Cross-sectional morphology of bondcoat samples after oxidation for 200 h at 1200 °C (a) as-sprayed sample, (b) Al coated sample; and EDX spectrum (c) point A, (d) point B, (e) point C, and (f) point D.

**Table 4.** Compositions data measured by EDX on the cross-section of as-sprayed and Al coated NiCrAlY samples after oxidation for 200 h at 1200 °C.

Composition (wt.%)	As-Sprayed Sample		Al Coated Sample	
	Site A	Site B	Site C	Site D
Al	80	28	85	18
Cr	14	60	10	72
Ni	6	12	5	10

In both samples, the TGO scales consist of a dark inner layer and a bright outer layer. Besides, some pores and voids are observed in the outer layer in both bondcoat samples. EDX data show that Al content is 80 and 85 wt.% at sites A and C, respectively. This indicates that the inner layers of oxides in both samples are  $\alpha$ - $\text{Al}_2\text{O}_3$  layers. On the other hand, Cr content at site B and D is 60 and 72 wt.%, respectively, which means that the outer layers of oxides consist of  $\text{Cr}_2\text{O}_3 + \text{Ni}(\text{Al,Cr})_2\text{O}_4$  mixed oxides [18,22,24,27].

Since the TGOs are non-uniformly distributed on the surface of both bondcoat samples, the thickness of the TGO of as-sprayed bondcoat sample is in the range of  $\sim 6.3$  to  $\sim 20.2$   $\mu\text{m}$ , while the thickness of the TGO of Al coated bondcoat sample is in the range of  $\sim 3.6$  to  $\sim 15.3$   $\mu\text{m}$ . Moreover, the average thickness of the TGO of as-sprayed sample is  $\sim 17.2$   $\mu\text{m}$ , in which the average thickness of  $\alpha$ - $\text{Al}_2\text{O}_3$  layer is  $< 2.0$   $\mu\text{m}$ . For Al coated bondcoat sample, the average thickness is  $\sim 7.4$   $\mu\text{m}$ , while the average thickness of  $\alpha$ - $\text{Al}_2\text{O}_3$  layer is  $\sim 3.3$   $\mu\text{m}$ .

Figure 8 shows the average thickness of oxides as a function of oxidation time for as sprayed sample (Figure 8a) and Al coated sample (Figure 8b). For both samples, the thickness of oxides increases with prolonged oxidation time. At both 5 h and 200 h, the thickness of oxides in the as-sprayed sample is larger than that of oxides in Al coated sample.

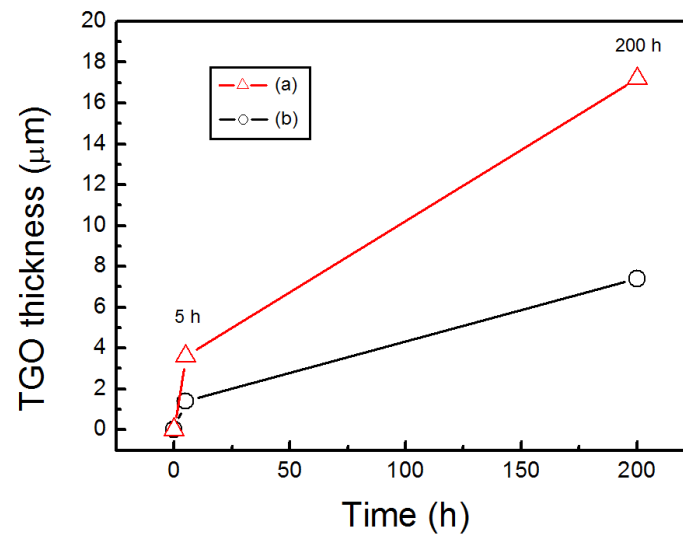


**Figure 8.** TGO thickness as a function of oxidation time for (a) as sprayed sample, and (b) Al coated sample.

#### 3.4. Thermal Cycling Oxidation Behavior of NiCrAlY Bondcoat Samples

Cyclic oxidation was conducted at 1050 °C. NiCrAlY bondcoat samples before and after Al deposition treatment were studied as a function of oxidation time. In Figure 9, the curve 9a and 9b show the weight gain per unit area as a function of oxidation time ( $\Delta M/S$  vs. time) for as-sprayed and Al coated NiCrAlY bondcoat samples, respectively. It can be found that the  $\Delta M/S$  of Al coated bondcoat samples is lower than that of as-sprayed bondcoat samples. In addition, the oxidation rate of the samples was calculated by ratioing the weight gain per unit area at 204 h to the longest oxidation time during the experiment, i.e., 204 h. The oxidation rate of as-sprayed and Al coated samples are  $3.4 \times 10^{-4}$  and  $1.7 \times 10^{-4}$   $\text{mg}\cdot\text{cm}^{-2}\cdot\text{h}^{-1}$  respectively. This result is in agreement with the results obtained in isothermal oxidation.

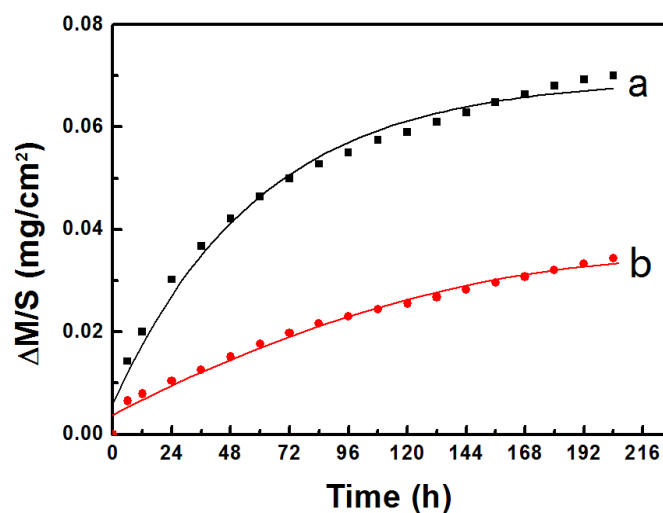


**Figure 9.** Weight gain of bondcoat samples as a function of oxidation time for (a) as-sprayed sample, (b) Al coated sample. The cyclic oxidation was carried out at 1050 °C for 204 h.

#### 4. Discussion

Figure 10a,b shows the schematics of oxidation process of as-sprayed and Al coated NiCrAlY bondcoat samples, respectively. Figure 10 illustrates the effect of Al sputtering treatment on the oxidation behavior of NiCrAlY bondcoat.

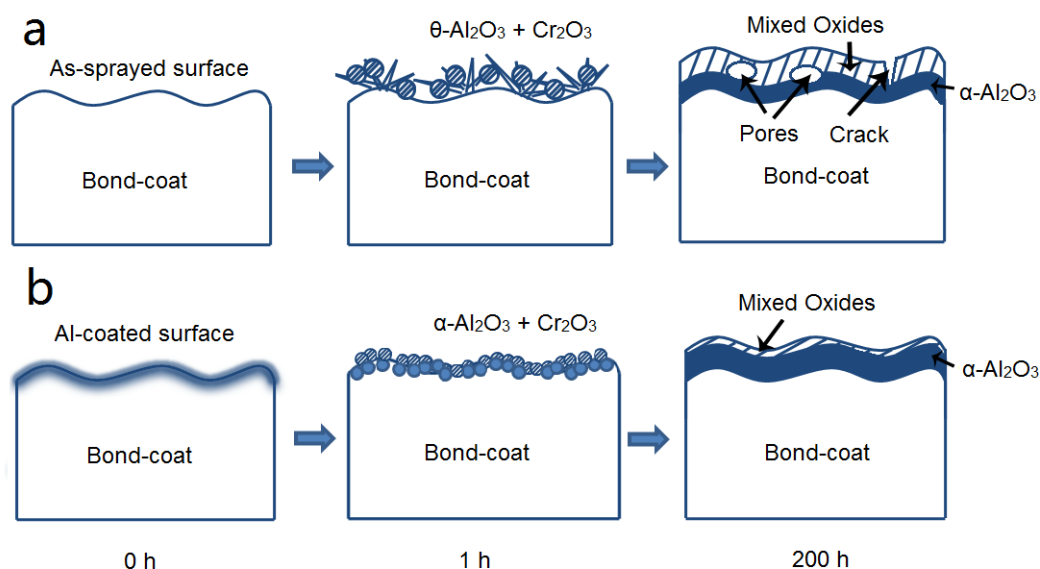


**Figure 10.** Schematic diagram illustrating the isothermal oxidation behavior of bondcoat samples oxidized at 1200 °C for 200 h (a) as-sprayed sample, (b) Al coated sample.

In 0 h state, the morphologies of as-sprayed and Al coated NiCrAlY bondcoat samples are similar. EDX line scan of Figure 2 and EDX mapping of Figure 3 shows that the Al film is successfully deposited on the surface of NiCrAlY bondcoat. It was reported that  $\alpha$ -Al<sub>2</sub>O<sub>3</sub> is more stable than  $\theta$ -Al<sub>2</sub>O<sub>3</sub> [25]. Therefore, with higher temperature, larger Al content, or longer oxidation time, either  $\alpha$ -Al<sub>2</sub>O<sub>3</sub> forms without  $\theta$ -Al<sub>2</sub>O<sub>3</sub> or the  $\theta$ -Al<sub>2</sub>O<sub>3</sub> phase transform to  $\alpha$ -Al<sub>2</sub>O<sub>3</sub> phase [25,26]. In addition, after the formation of continuous  $\alpha$ -Al<sub>2</sub>O<sub>3</sub> layer during oxidation at high temperature, the oxidation process of bondcoat is dramatically slowing down [24–27]. This is due to the fact that  $\alpha$ -Al<sub>2</sub>O<sub>3</sub> has slower growth rate compared to other oxides such as Cr<sub>2</sub>O<sub>3</sub> and NiO [32,33]. Thus, higher Al content in NiCrAlY bondcoat are reported to prevent the formation of metastable aluminas and mixed oxides [24,27,32,33]. This leads to the longer lifetime of bondcoat samples in severe environments [37–39].

The Cr<sub>2</sub>O<sub>3</sub> phase is observed and detected on both as-sprayed and Al coated NiCrAlY bondcoat samples, after isothermal oxidation at 1200 °C for 1 h (Figure 10a,b). The formation of Cr<sub>2</sub>O<sub>3</sub> phase is due to the high inter-diffusion coefficient and the high concentration of Cr. In addition, the depletion of Al resulted from the oxidation during the APS process also leads to the formation of Cr<sub>2</sub>O<sub>3</sub> phase [40–42].

After isothermal oxidation for 1 h at 1200 °C, whisker-like  $\theta$ -Al<sub>2</sub>O<sub>3</sub> formed on the surface of as-sprayed bondcoat samples, while dense equiaxed structure  $\alpha$ -Al<sub>2</sub>O<sub>3</sub> oxides can be found on the surface of Al coated samples. Oxides of  $\theta$ -Al<sub>2</sub>O<sub>3</sub> are prone to grow on the bondcoat surface, which possesses a relatively low Al content [40–43]. On the surface of Al coated samples, higher Al content is achieved. Besides, the activity of Al is higher than that of Cr and Ni. Therefore, when the Al coated bondcoat is exposed to the air, Al is in favor of diffusion into the surface area [41–43]. The results are consistent with the earlier study from Nijdam et al. [42,43]. In the initial stages (<1 h) of oxidation, the quantity of Al oxides rapidly increases on the NiCrAl alloys surface.

Moreover, the difference between as-sprayed bondcoat sample and Al coated sample is that as-sprayed sample has a free surface, while Al coated sample is lack of the free surface. This may affect the Al in bondcoat diffusing upward towards the surface. A possible mechanism is proposed. During the initial oxidation process, excessive levels of oxygen are available on the surface area of bondcoat samples. For the Al coated sample, the Al in Al layer reacts with the oxygen and forms a thin layer of  $\alpha$ -Al<sub>2</sub>O<sub>3</sub> oxides, which can slow down the Al diffusion upward from bondcoat. While for as-sprayed sample, the Al in bondcoat tends to diffuse to the surface reacting with oxygen from the onset due to high activity compared with Ni and Cr in bondcoat. However, the formation time for  $\alpha$ -Al<sub>2</sub>O<sub>3</sub> layer in as-sprayed sample is slower than that in Al coated sample.

After isothermal oxidation for 200 h at 1200 °C, both as-sprayed and Al coated NiCrAlY bondcoat samples form TGO, which consisted of two layers, i.e., the inner layer of dark  $\alpha$ -Al<sub>2</sub>O<sub>3</sub> and the outer layer of bright mixed oxides (Cr<sub>2</sub>O<sub>3</sub> + Ni(Al,Cr)<sub>2</sub>O<sub>4</sub>). The oxides layer distribution is in agreement with earlier studies [18,22,33,38,40,41]. From the thermodynamics point of view, the formation of  $\alpha$ -Al<sub>2</sub>O<sub>3</sub> layer is due to the fact that Al is a probable element in the bondcoat, which is prone to react with oxygen at the initial stage of oxidation [37]. After the depletion of Al occurs, Cr<sub>2</sub>O<sub>3</sub> phase form in the bondcoat. This is because of the large content of Cr element (20 wt.%) and the high inter-diffusion coefficient characteristic of Cr [38]. Owing to the low diffusivity and solubility of oxygen in the NiCrAlY bondcoats, the diffusion of Cr is from the deep part to the surface, thus internal Cr<sub>2</sub>O<sub>3</sub> oxides are not formed in the samples [40]. Ni diffuses through the microcracks in Al<sub>2</sub>O<sub>3</sub> and Cr<sub>2</sub>O<sub>3</sub> phases, which reacts with Cr and Al on the surface of bondcoats, forming the spinel oxides. Based on this mechanism, after isothermal oxidation for 200 h, the two-layer structure of oxides was observed.

A part of the  $\alpha$ -Al<sub>2</sub>O<sub>3</sub> layer formed in the as-sprayed samples is from the  $\theta$ -Al<sub>2</sub>O<sub>3</sub> to  $\alpha$ -Al<sub>2</sub>O<sub>3</sub> phase transformation during the isothermal oxidation process [25,26,33]. The volume expansion (12%) is accompanied with the phase transformation from  $\theta$ -Al<sub>2</sub>O<sub>3</sub> to  $\alpha$ -Al<sub>2</sub>O<sub>3</sub> [2,25–27]. This leads to the formation of some pores and cracks in the  $\alpha$ -Al<sub>2</sub>O<sub>3</sub> layer in as-sprayed samples, while a dense  $\alpha$ -Al<sub>2</sub>O<sub>3</sub> layer is observed in the Al coated samples. For Al sputtered samples, the formation of an intact  $\alpha$ -Al<sub>2</sub>O<sub>3</sub> layer barrier is helpful to prevent the formation of spinel oxides during the isothermal oxidation; while for as-sprayed samples, the formation of pores and cracks in the spinel oxides accelerates the oxygen attack and leads to the non-uniform TGO. Therefore, a thinner and finer TGO is observed in the Al coated samples as compared to the as-sprayed samples [44,45]. The results from isothermal oxidation in Figure 8 and cyclic oxidation in Figure 9 also demonstrate that the as-sprayed samples possess a larger weight gain per unit area than that of the Al coated samples, indicating a better oxidation resistance of Al coated samples.

One major flaw of this study is that the obtained results are not in the context of TBCs, but in the bondcoat samples without topcoat. This is related not only to the oxidation kinetics, but also to the interaction among the bondcoat fractal roughness, biaxial TGO stresses, and the elastic properties of ceramic topcoats. Over the years, studies found that investigating on the oxidation kinetics of thermal sprayed bondcoats exclusively without its interaction with topcoats does not give a clear picture of its effects on TBC lifetime [46–50]. Therefore, the design of experiments could be improved in the future work.

## 5. Conclusions

In this study, dense and continuous Al film (thickness = ~2.0  $\mu$ m) was successfully sputtered on the surface of NiCrAlY bondcoat. This Al film improved the oxidation resistance of the NiCrAlY bondcoat.

- The isothermal oxidation of Al coated bondcoat samples under 1200 °C for 1 h led to the formation of  $\alpha$ -Al<sub>2</sub>O<sub>3</sub> and Cr<sub>2</sub>O<sub>3</sub>. Under the same oxidation conditions,  $\theta$ -Al<sub>2</sub>O<sub>3</sub> and Cr<sub>2</sub>O<sub>3</sub> formed on the surface of as-sprayed bondcoat samples. This indicated that enhanced Al content suppressed the formation of metastable aluminas.
- After isothermally oxidized at 1200 °C for 200 h, the TGO layers formed on the surface of Al coated and as-sprayed bondcoat samples. TGOs consisted of a bright outer mixed oxides layer and a dark inner  $\alpha$ -Al<sub>2</sub>O<sub>3</sub> layer. The average thickness of the TGO of as-sprayed samples was ~17.2  $\mu$ m; while that of Al coated samples was ~7.4  $\mu$ m. The average thickness of  $\alpha$ -Al<sub>2</sub>O<sub>3</sub> layer in as-sprayed samples was <2.0  $\mu$ m, while that of Al coated samples was ~3.3  $\mu$ m. This indicated that a finer TGO formed after increasing the Al content on the surface of bondcoat.
- Cyclic oxidation was performed at 1050 °C for 204 h. Results showed that the weight gain per unit area of Al coated bondcoat samples was smaller than that of as-sprayed bondcoat samples. Thus, better oxidation resistance was achieved by Al sputtering.

In the coming study, more complicated structural thermal barrier coatings are planned to be produced using the sputtering method, such as functional graded coatings. However, the balance between composition improvement and mechanical properties of the coatings should be carefully investigated.

**Author Contributions:** Conceptualization, Y.Z. and C.Z.; methodology, G.Z.; software, Q.Y.; validation, Q.Y., W.C. and J.P.; formal analysis, Y.Z. and G.Z.; investigation, G.Z.; writing—original draft preparation, Y.Z.; writing—review and editing, C.Z. and J.P.; supervision, C.Z. All authors have read and agreed to the published version of the manuscript.

**Funding:** This research was funded by the Science and Technology Program of Shaanxi Province, grant number 2020GY-278 and 2020ZDLGY12-07; the Special Fund for Basic Scientific Research of Central Colleges, Xi'an, China, grant number 300102318206; the Chinese Natural Science Foundation, grant number 51301023 and 51401170; and the State Key Laboratory of Materials Processing and Die & Mould Technology, Huazhong University of Science and Technology, Hangzhou, China, grant number P2016-13.

**Conflicts of Interest:** The authors declare no conflict of interest.

## References

1. Padture, N.P.; Gell, M.; Jordan, E.H. Thermal barrier coatings for gas-turbine engine applications. *Science* **2002**, *296*, 280–284. [[CrossRef](#)]
2. Clarke, D.R.; Levi, C.G. Materials design for the next generation thermal barrier coatings. *Annu. Rev. Mater. Res.* **2003**, *33*, 383–417. [[CrossRef](#)]
3. Zhang, P.; Zhang, X.; Li, F.; Zhang, Z.; Li, H.; Wang, Y.; Ren, L.; Liu, M. Effects of selective laser modification and Al deposition on the hot corrosion resistance of ceria and yttria-stabilized zirconia thermal barrier coatings. *Coatings* **2019**, *9*, 353. [[CrossRef](#)]
4. Song, D.; Song, T.; Paik, U.; Lyu, G.; Jung, Y.G.; Choi, B.G.; Kim, I.S.; Zhang, J. Crack-growth behavior in thermal barrier coatings with cyclic thermal exposure. *Coatings* **2019**, *9*, 365. [[CrossRef](#)]
5. Cao, X.Q.; Vassen, R.; Stover, D. Ceramic materials for thermal barrier coatings. *J. Eur. Ceram. Soc.* **2004**, *24*, 1–10. [[CrossRef](#)]
6. Vassen, R.; Stuke, A.; Stover, D. Recent developments in the field of thermal barrier coatings. *J. Therm. Spray Technol.* **2009**, *18*, 181–186. [[CrossRef](#)]
7. Bumgardner, C.; Croom, B.; Li, X. High-temperature delamination mechanisms of thermal barrier coatings. *Acta Mater.* **2017**, *128*, 54–63. [[CrossRef](#)]
8. Meng, G.H.; Zhang, B.Y.; Sun, X.G.; Pan, Z.Y.; He, G.Q.; Zhou, Y.; Wu, P.L. Vacuum heat treatment mechanisms promoting the adhesion strength of thermally sprayed metallic coatings. *Surf. Coat. Technol.* **2018**, *344*, 102–110. [[CrossRef](#)]
9. Mahalingam, S.; Yunus, S.M.; Li, F.; Manap, A.; Afandi, N.M.; Zainuddin, R.A.; Kadir, N.F. Crack propagation and effect of mixed oxides on TGO growth in thick La–Gd–YSZ thermal barrier coating. *Coatings* **2019**, *9*, 719. [[CrossRef](#)]
10. Feng, J.; Ren, X.; Wang, X.; Zhou, R.; Pan, W. Thermal conductivity of ytterbia-stabilized zirconia. *Scripta Mater.* **2012**, *66*, 41–44. [[CrossRef](#)]
11. Cordier, A.; El Khal, H.; Siebert, E.; Steil, M.C. On the role of the pore morphology on the electrical conductivity of porous yttria-stabilized zirconia. *J. Eur. Ceram. Soc.* **2019**, *39*, 2518–2525. [[CrossRef](#)]
12. Ozgurluk, Y.; Doleker, K.M.; Ozkan, D.; Ahlatci, H.; Karaoglanli, A.C. Cyclic hot corrosion failure behaviors of EB-PVD TBC systems in the presence of sulfate and vanadate molten salts. *Coatings* **2019**, *9*, 166. [[CrossRef](#)]
13. Lima, R.S.; Guerreiro, B.M.H.; Aghasibeig, M. Microstructural Characterization and Room-Temperature Erosion Behavior of As-Deposited SPS, EB-PVD and APS YSZ-Based TBCs. *J. Therm. Spray Technol.* **2019**, *28*, 223–232. [[CrossRef](#)]
14. Saldaña, J.M.; Schulz, U.; Rodríguez, G.C.M.; Cacerse-Díaz, L.A.; Lau, H. Microstructure and lifetime of Hf or Zr doped sputtered NiAlCr bond coat/7YSZ EB-PVD TBC systems. *Surf. Coat. Technol.* **2018**, *335*, 41–51. [[CrossRef](#)]
15. Meng, G.H.; Liu, H.; Liu, M.J.; Xu, T.; Yang, G.J.; Li, C.X.; Li, C.J. Highly oxidation resistant MCrAlY bond coats prepared by heat treatment under low oxygen content. *Surf. Coat. Technol.* **2019**, *368*, 192–201. [[CrossRef](#)]

16. Meng, G.H.; Zhang, B.Y.; Liu, H.; Yang, G.J.; Xu, T.; Li, C.X.; Li, C.J. Highly oxidation resistant and cost effective MCrAlY bond coats prepared by controlled atmosphere heat treatment. *Surf. Coat. Technol.* **2018**, *347*, 54–65. [[CrossRef](#)]
17. Zhao, X.; Xiao, P. Thermal barrier coatings on nickel superalloy substrates. *Sci. Forum* **2009**, *606*, 1–26. [[CrossRef](#)]
18. Zhu, C.; Li, P.; Javed, A.; Liang, G.Y.; Xiao, P. An investigation on the microstructure and oxidation behavior of laser remelted air plasma sprayed thermal barrier coatings. *Surf. Coat. Technol.* **2012**, *206*, 3739–3746. [[CrossRef](#)]
19. Tolpygo, V.K.; Clarke, D.R. Surface rumpling of a (Ni, Pt) Al bond coat induced by cyclic oxidation. *Acta Mater.* **2000**, *48*, 3283–3293. [[CrossRef](#)]
20. Parlikar, C.; Alam, M.Z.; Chatterjee, D.; Das, D.K. Oxidation and concomitant effects on the microstructure and high temperature tensile properties of a DS Ni-base superalloy applied with different thicknesses of Pt-aluminide (PtAl) bond coat. *Surf. Coat. Technol.* **2019**, *373*, 25–37. [[CrossRef](#)]
21. Lu, Z.; Lyu, G.; Gulhane, A.; Park, H.M.; Kim, J.S.; Jung, Y.J.; Zhang, J. Experimental and modeling studies of bond coat species effect on microstructure evolution in EB-PVD thermal barrier coatings in cyclic thermal environments. *Coatings* **2019**, *9*, 626. [[CrossRef](#)]
22. Zhu, C.; Javed, A.; Li, P.; Yang, F.; Liang, G.Y.; Xiao, P. A study of the microstructure and oxidation behavior of alumina/yttria-stabilized zirconia (Al<sub>2</sub>O<sub>3</sub>/YSZ) thermal barrier coatings. *Surf. Coat. Technol.* **2012**, *206*, 214–222. [[CrossRef](#)]
23. Zhang, B.Y.; Meng, G.H.; Yang, G.J.; Li, C.X.; Li, C.J. Dependence of scale thickness on the breaking behavior of the initial oxide on plasma spray bond coat surface during vacuum pre-treatment. *Appl. Surf. Sci.* **2017**, *397*, 125–132. [[CrossRef](#)]
24. Xu, S.Q.; Zhu, C.; Zhang, Y. Effects of laser remelting and oxidation on NiCrAlY/8Y<sub>2</sub>O<sub>3</sub>-ZrO<sub>2</sub> thermal barrier coatings. *J. Therm. Spray Technol.* **2018**, *27*, 412–422. [[CrossRef](#)]
25. An, T.F.; Guan, H.R.; Sun, X.F.; Hu, Z.Q. Effect of the  $\theta$ - $\alpha$ -Al<sub>2</sub>O<sub>3</sub> transformation in scales on the oxidation behavior of a nickel-base superalloy with an aluminide diffusion coating. *Oxid. Met.* **2000**, *54*, 301–316. [[CrossRef](#)]
26. Puetz, P.; Huang, X.; Yang, Q.; Tang, Z. Transient oxide formation on APS NiCrAlY after oxidation heat treatment. *J. Therm. Spray Technol.* **2011**, *20*, 621–629. [[CrossRef](#)]
27. Zhu, C.; Li, P.; Wu, X.Y. A study of the diffusion and pre-oxidation treatment on the formation of Al<sub>2</sub>O<sub>3</sub> ceramic scale on NiCrAlY bond-coat during initial oxidation process. *Ceram. Int.* **2016**, *42*, 7708–7716. [[CrossRef](#)]
28. Niranatumpom, P.; Ponton, C.B.; Evans, H.E. The failure of protective oxides on plasma-sprayed NiCrAlY overlay coatings. *Oxid. Met.* **2000**, *53*, 241–258. [[CrossRef](#)]
29. Swadzba, R. Interfacial phenomena and evolution of modified aluminide bondcoatings in thermal barrier coatings. *Appl. Surf. Sci.* **2018**, *445*, 133–144. [[CrossRef](#)]
30. Zhang, B.Y.; Shi, J.; Yang, G.J.; Li, C.X.; Li, C.J. Healing of the interface between splashed particles and underlying bulk coating and its influence on isothermal oxidation behavior of LPPS MCrAlY bond coat. *Therm. Spray Technol.* **2015**, *24*, 611–621. [[CrossRef](#)]
31. Goward, G.W. Progress in coatings for gas turbine airfoils. *Surf. Coat. Technol.* **1998**, *108–109*, 73–79. [[CrossRef](#)]
32. Brossard, J.M.; Balmain, J.; Sanchette, F.; Bonnet, G. High-temperature oxidation of an aluminized NiCr alloy formed by a magnetron-sputtered Al diffusion coating. *Oxid. Met.* **2005**, *64*, 43–61. [[CrossRef](#)]
33. Zhu, C.; Javed, A.; Li, P.; Liang, G.Y.; Xiao, P. Study of the effect of laser treatment on the initial oxidation behaviour of Al-coated NiCrAlY bond-coat. *Surf. Interface Anal.* **2013**, *45*, 1680–1689. [[CrossRef](#)]
34. Zhang, P.P.; Li, F.H.; Zhang, X.F.; Zhang, Z.H.; Zhou, F.F.; Ren, L.Q.; Liu, M. Thermal shock resistance of thermal barrier coatings with different surface shapes modified by laser remelting. *J. Therm. Spray Technol.* **2019**, *28*, 417–432. [[CrossRef](#)]
35. Haynes, J.A.; Unocic, K.A.; Pint, B.A. Effect of water vapor on the 1100°C oxidation behavior of plasma-sprayed TBCs with HVOF NiCoCrAlX bond coatings. *Surf. Coat. Technol.* **2013**, *215*, 39–45. [[CrossRef](#)]
36. Strawbridge, A.; Evans, H.E.; Ponton, C.B. Spallation of oxide scales from NiCrAlY overlay coatings. *Mater. Sci. Forum.* **2009**, *251–254*, 365–372. [[CrossRef](#)]
37. Nijdam, T.J.; Jeurgens, L.P.H.; Sloof, W.G. Promoting exclusive  $\alpha$ -Al<sub>2</sub>O<sub>3</sub> growth upon high-temperature oxidation of NiCrAl alloys: Experiment versus model predictions. *Acta Mater.* **2005**, *53*, 1643–1653. [[CrossRef](#)]

38. Chen, W.R.; Archer, R.; Huang, X.; Marple, B.R. TGO growth and crack propagation in a thermal barrier coating. *J. Therm. Spray Technol.* **2008**, *17*, 858–864. [[CrossRef](#)]
39. Nijdam, T.J.; Sloof, W.G. Modelling of composition and phase changes in multiphase alloys due to growth of an oxide layer. *Acta Mater.* **2008**, *56*, 4972–4983. [[CrossRef](#)]
40. Chen, W.R.; Wu, X.; Dudzinski, X. Influence of thermal cycle frequency on the TGO growth and cracking behaviors of an APS-TBC. *J. Therm. Spray Technol.* **2012**, *21*, 1294–1299. [[CrossRef](#)]
41. Chen, W.R. Degradation of a TBC with HVOF-CoNiCrAlY bond coat. *J. Therm. Spray Technol.* **2014**, *23*, 876–884. [[CrossRef](#)]
42. Nijdam, T.J.; Marijnissen, G.H.; Vergeldt, E.; Kloosterman, A.B.; Sloof, W.G. Development of a pre-oxidation treatment to improve the adhesion between thermal barrier coatings and NiCoCrAlY bond coatings. *Oxid. Met.* **2006**, *66*, 269–294. [[CrossRef](#)]
43. Nijdam, T.J.; Sloof, W.G. Combined pre-annealing and pre-oxidation treatment for the processing of thermal barrier coatings on NiCoCrAlY bond coatings. *Surf. Coat. Technol.* **2006**, *201*, 3894–3900. [[CrossRef](#)]
44. Evans, A.G.; Clarke, D.R.; Levi, C.G. The influence of oxides on the performance of advanced gas turbines. *J. Eur. Ceram. Soc.* **2008**, *28*, 1405–1419. [[CrossRef](#)]
45. Yang, G.J.; Xiang, X.D.; Xing, L.K.; Li, D.J.; Li, C.X.; Li, C.J. Isothermal oxidation behavior of NiCoCrAlTaY coating deposited by high velocity air-fuel spraying. *J. Therm. Spray Technol.* **2012**, *21*, 391–399. [[CrossRef](#)]
46. Haynes, J.A.; Pint, B.A.; Porter, W.D.; Wright, I.G. Comparison of thermal expansion and oxidation behavior of various high-temperature coating materials and superalloys. *Mater. High Temp.* **2004**, *21*, 87–94. [[CrossRef](#)]
47. Weeks, M.D.; Subramanian, R.; Vaidya, A.; Mumm, D.R. Defining optimal morphology of the bond coat–thermal barrier coating interface of air-plasma sprayed thermal barrier coating systems. *Surf. Coat. Technol.* **2015**, *273*, 50–59. [[CrossRef](#)]
48. Lance, M.J.; Haynes, J.A.; Pint, B.A. The effects of temperature and substrate curvature on TBC lifetime and residual stress in alumina scales beneath APS YSZ. *Surf. Coat. Technol.* **2016**, *308*, 19–23. [[CrossRef](#)]
49. Gildersleeve, V.E.; Viswanathan, V.; Lance, M.J.; Haynes, J.A.; Pint, B.A.; Sampath, S. Role of bond coat processing methods on the durability of plasma sprayed thermal barrier systems. *Surf. Coat. Technol.* **2019**, *375*, 782–792. [[CrossRef](#)]
50. Kane, K.A.; Lance, M.J.; Sweet, M.; Pint, B.A. The effect of bond coating surface modification on the performance of atmospheric plasma spray thermal barrier coatings. *Surf. Coat. Technol.* **2019**, *378*, 125042. [[CrossRef](#)]



© 2020 by the authors. Licensee MDPI, Basel, Switzerland. This article is an open access article distributed under the terms and conditions of the Creative Commons Attribution (CC BY) license (<http://creativecommons.org/licenses/by/4.0/>).